Solar Energy Materials and Solar Cells 195 (2019) 213–219

Contents lists available at ScienceDirect

Solar Energy Materials and Solar Cells

journal homepage: www.elsevier.com/locate/solmat

The use of HfO_2 in a point contact concept for front interface passivation of $Cu(In,Ga)Se_2$ solar cells

Johannes Löckinger[a,*], Shiro Nishiwaki[a], Benjamin Bissig[a], Giedrius Degutis[b], Yaroslav E. Romanyuk[a], Stephan Buecheler[a], Ayodhya N. Tiwari[a]

[a] Laboratory for Thin Films and Photovoltaics, Empa - Swiss Federal Laboratories for Materials Science and Technology, Überlandstrasse 129, 8600 Dübendorf, Switzerland
[b] Institute for Materials Research (IMO), Hasselt University, B-3500, Hasselt, Belgium

ARTICLE INFO

Keywords:
$Cu(In,Ga)Se_2$ solar cell
CIGS
HfO_2
Point contact
Passivation
ALD

ABSTRACT

We report on the use of a high bandgap metal-oxide at the front interface of $Cu(In,Ga)Se_2$ (CIGS) solar cells in a point contact concept for reduced interface recombination. Highly resistive HfO_2 is applied on the CIGS surface by atomic layer deposition (ALD). Aspects of the surface passivating effect of HfO_2 on CIGS were investigated by time-resolved photoluminescence (TRPL), electron beam induced current (EBIC) and capacitance-voltage (C-V) measurements. Two structuring methods for point contact formation are compared, a lithographic top-down and a simple bottom-up approach using NaCl as template. The former method employed a plasma etch step which was found to degrade the performance of solar cells when applied on the CIGS surface. The template method omitted sputtering and allowed patterning of HfO_2 up to 10 nm thickness without adversely impacting the open-circuit voltage (V_{OC}). EBIC revealed an improved carrier collection due to the HfO_2 coating and a long term stable PL decay was observed. Yet, the point contact concept with HfO_2 was not significantly influencing the performance of a CIGS solar cell for the investigated parameter range.

1. Introduction

Photovoltaic (PV) devices based on chalcogenide $Cu(In,Ga)Se_2$ (CIGS) absorber layers are among the most promising thin-film PV technologies reaching power conversion efficiencies (PCE) of 20.4% and 23.35% on flexible and rigid substrates [1,2]. The highest device efficiencies were achieved on CIGS absorbers which were subjected to a post deposition treatment (PDT), whereby an additional evaporation of heavy alkali (K, Rb, Cs) fluorides after a NaF treatment is significantly improving device performance [3]. Also, the strong variations in device performance depending on which and how the buffer layer – CdS, Zn(S,O), Zn_xMg_yO, In_xS_y, Zn_xSn_yO – is applied suggests that the front CIGS/buffer interface is crucial for achieving a high PCE [4].

The concept of using high band gap dielectrics to passivate the front surface with point contacts was successfully developed in Si solar cells with the PERC (passivated emitter and rear cell) structure [5]. Both Al_2O_3 and HfO_2 have shown both chemical and field-effect passivation qualities in Si solar cells [6,7]. Similar considerations motivated the point contact concept for reduced interface recombination in CIGS solar cells at both the rear and front interface. At the rear contact, i.e. at the Mo/CIGS interface, ALD-Al_2O_3 with nanosized openings was successfully applied for thin (< 1.5 µm) absorber layers [8–12]. For an effective field assisted passivation at the front CIGS interface a positive coulombic charge (repelling holes) is assumed to be beneficial, opposite to what has been suggested for the rear interface by Kotipalli et al. [13]. For Al_2O_3 on CIGS a negative effective charge density (Q_{eff}) was determined by CV-measurements on metal-insulator-semiconductor (MIS) structures for a range of CIGS electron affinities (χ) of 3.9–4.5 eV [13]. While for HfO_2 both a negative or positive Q_{eff} was reported, depending on the magnitude of χ_{CIGS} [14].

A simulation-based study by Sozzi et al. [15] explored the prerequisites for a successful point contact concept at the front interface. They found a strong dependence of the I-V parameters on the geometry of the point contacts (i.e. size and spacing) in the highly resistive oxide layer. Hence the structuring method is expected to play a critical role for this concept, especially on the CIGS surface.

Several approaches for the formation of point contacts have been established, most of them are based on lithographic processing or template approaches. The lithographic methods usually involve the deposition a photoresist which is masked, developed and plasma etched together with the underlying oxide layer. This method has been applied e.g. for Al_2O_3 coated Mo as the rear contact of CIGS solar cells [12]. Template approaches involve the application of e.g. SiO_2, CdS or Mo

* Corresponding author.
E-mail address: johannes.loeckinger@empa.ch (J. Löckinger).

https://doi.org/10.1016/j.solmat.2019.03.009
Received 25 January 2019; Received in revised form 2 March 2019; Accepted 4 March 2019
Available online 16 March 2019

nanospheres for the structuring of Al_2O_3 at either rear or front contact [10,16,17].

Point contacts with a regular spacing are more difficult to achieve at the front interface as compared to the rear due to the surface roughness of CIGS. Hultqvist et al. [16] have shown that structuring of a resistive oxide layer on the front CIGS surface by nanosphere lithography is possible and that Al_2O_3 is able to improve the device performance compared to a buffer-less device. However, compared to a reference structure with a CdS buffer layer, however, the PCE is significantly lower (~50%).

This report investigates HfO_2 as high band gap dielectric (E_g ~ 5.6 eV [18]) in a point contact concept at the front CIGS interface. Two structuring procedures were tested, a lithographic and a template-based method. Due to its chemical inertness HfO_2 can be used in combination with a CBD-CdS, and solar cells with a structured HfO_2 added to the otherwise standard device structure are processed. The passivating effect of ALD-HfO_2 on the front CIGS surface is evaluated by C-V, TRPL and EBIC measurements.

In the last part the template structuring method is used to insert a thin HfO_2 layer in between the buffer and window layer to address potential sputtering damage of the window layer deposition.

2. Experimental section

2.1. Sample fabrication

Both MIS devices and solar cells were produced. The general device architecture in case of a MIS device is SLG/SiOx/Mo/CIGS/HfO_2/Al. For solar cells the following two structures were investigated: SLG/SiOx/Mo/CIGS/HfO_2/CdS/ZnO/Al:ZnO and SLG/SiOx/Mo/CIGS/CdS/HfO_2/ZnO/Al:ZnO with the respective reference structures omitting the HfO_2 layer.

CIGS was deposited by elemental co-evaporation from effusion cells on SiO_x and Mo coated soda lime glass (SLG) substrates. The base pressure of the deposition chamber was ~10^{-7} mbar. A multi-stage process was used with either a [Ga]/([Ga]+[In]) (GGI) grading or with a constant GGI (ungraded) as reported before [19]. The absorber layer composition was measured by x-ray fluorescence (XRF). The [Cu]/([In]+[Ga]) (CGI) ratio and the GGI is stated for the respective experiment. A NaF PDT was performed as described in Ref. [20]. The absorber layer thickness was between 2.5 and 3 µm as determined by scanning electron microscopy (SEM). A ~50 nm thick CdS layer was deposited by chemical bath deposition (CBD) from cadmium acetate (2.3 mM), thiourea (22 mM) and ammonium hydroxide (2 M [NH3]) at 70 °C. A post deposition annealing at 180 °C for 2 min in air was performed directly after the CBD.

ZnO (~80 nm) was deposited by rf-magnetron sputtering in an Ar/O2 (0.02%) atmosphere at a pressure of 0.46 Pa with a power density of 1.9 W cm^{-2}

HfO_2 was deposited by ALD at a substrate temperature of 220 °C (when deposited on ungraded absorbers) or 175 °C (for graded absorbers, to limit any annealing effects) with Ar as carrier gas at a base pressure of 13 Pa in a Fiji G2 system (Ultratech). For samples where CdS was already deposited prior to the ALD process the temperature for the HfO_2 deposition was reduced to 120 °C (to avoid annealing effects reported e.g. by Koprek et al. [21]). The precursors were tetrakis(dimethylamino)hafnium(IV) (TDMAH, Merck, 4 N+) or trimethylaluminium (TMA, Merck, 97%) (for the deposition of Al_2O_3) and H_2O. TDMAH was kept at 75 °C while TMA and H_2O were unheated. The growth rate was determined by ellipsometry on Si (100) reference substrates and compared to SEM micrographs on CIGS. A linear growth rate of ~0.1 nm/cycle was observed.

Al:ZnO (2%$_{wt}$ Al_2O_3, 1.8 W cm^{-2}, ~150 nm) was deposited by magnetron sputtering. On top a Ni/Al grid (4 µm) was applied by e-beam evaporation. On some cells (as stated) 105 nm of MgF_2 were applied as anti-reflective coating. A cell area of 0.29 ± 0.03 cm^2 was defined by mechanical scribing.

2.2. Structuring of oxides

Either hole mask colloidal lithography (HCL) or a template approach with NaCl was used for the structuring of HfO_2. HCL is a top-down structuring approach, i.e. it is applied after the deposition of HfO_2 and hence allows to pattern even relatively thick oxide layers. The procedure involved the deposition of a photoresist (IX-845™), poly (diallyldimethylammonium chloride) PDDA and polystyrene (PS) beads (~100 nm) followed by a Cr mask evaporation. The PS beads are then removed by tape-stripping and the holes are etched by a 2-step plasma etching step consisting of O_2/Ar and SF_6 plasma. The PR is then removed by acetone in an ultrasonic bath. The alternative structuring method was performed as a bottom-up approach using NaCl as a template. The samples were dipped in a hot (~100 °C) saturated aqueous NaCl solution and dried with N_2. After the oxide deposition the samples were washed in an ultrasonic water bath for 3 min.

2.3. Characterization methods

Current-voltage (I-V) characteristics were measured with a Keithley 2400 source meter and four-terminal sensing under standard test conditions (AM1.5G, 298 K) using a type ABA solar simulator. For temperature dependent measurements a cryostat ($N_{2,l}$) equipped with a halogen lamp was used. External quantum efficiency (EQE) measurements were performed with a chopped halogen light source at 298 K and with ~100 W m^{-2} halogen light bias. The setup comprises further a tripple-grating monochromator and a Stanford Instruments lock-in amplifier. The probing light intensity was calibrated using a monocrystalline Si solar cell certified by Fraunhofer ISE. A Shimadzu UV-3600 spectrophotometer was used for transmission and reflectance measurements. SEM was performed on a Hitachi S-4800 electron microscope. Electron beam induced current (EBIC) and the secondary electron (SE) signal were simultaneously recorded with a commercially available system from GATAN. The procedure for sample preparation and measurement can be found in a previous report [22]. An Agilent E4980A LCR meter was used for capacitance measurements (C-f and C-V). Time-resolved photoluminescence (TRPL) measurements were performed with a 639 nm diode laser with a pulse duration of ~100 ps in combination with a InGaAs photomultiplier with time correlated single photon counting electronics. The pulse repetition rate was ~1 MHz. The typical photon density per pulse was around 7E+11 cm^{-2} as estimated from total laser power measurements with a spot size of about 50 µm.

3. Results and discussion

3.1. Characterization of test structures with uniform oxide layers

Fig. 1 shows the PL decays of three pieces of the same CIGS absorber with about 20 nm Al_2O_3 or HfO_2 deposited on top or the bare CIGS surface after a H_2O rinse. An ungraded CIGS absorber layer with a constant GGI (0.36) was used for this experiment to avoid carrier diffusion and recombination in the GGI grading minimum (“notch” region) which could reduce the effect of the surface recombination rate on the total recombination as recently observed [23]. Compared to the bare washed surface of the absorber an oxide layer, either Al_2O_3 or HfO_2, on top seems to prolong the PL decay in a similar way. This effect might not be solely ascribed to a reduced surface recombination rate since a strong annealing effect was observed and similar effective lifetimes (~20 ns) were obtained for all devices directly after a thermal treatment performed in the ALD reaction chamber in Ar at similar conditions (temperature, time, pressure) as the oxide layer deposition. The difference between the HfO_2 – and similarly Al_2O_3 – coated sample as compared to the bare absorber, is seen in terms of sample ageing. Re-measuring the bare absorber (uncoated) after a month stored under low vacuum conditions (< 1 mbar) showed a severe degradation in the PL

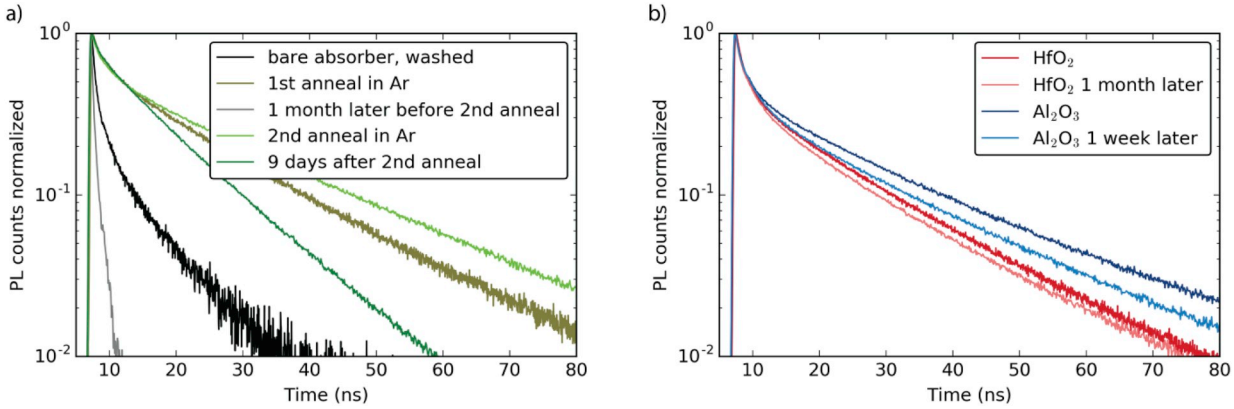

Fig. 1. Effects of ageing on the TRPL transients of an ungraded CIGS absorber (CGI = 0.84, GGI = 0.36). a) bare (uncoated) absorber after being washed in H_2O, annealed in Ar and stored in low vacuum (< 1 mbar). b) absorber coated with either HfO_2 or Al_2O_3 and stored in low vacuum. The background signal of each measurement is subtracted and the PL signal normalized.

decay which can be restored by annealing the device again. The annealing effect can therefore be seen as metastable and influencing rather the CIGS surface than the bulk. If HfO_2 is deposited on the CIGS surface, the PL decay remains stable even after a month of storage.

EBIC measurements were performed as a complementary approach to investigate effects of HfO_2 on the CIGS surface recombination (see Fig. 2). EBIC is an experimental approach to access the probability of collecting locally generated electrons which are injected by an electron beam into the CIGS cross section and measured as device current through the front and rear contacts. The procedure was in analogy to a report by Bissig et al. [22] that suggested the use of Al_2O_3 coating for a more accurate determination of the charge collection probability by EBIC measurements. A CIGS solar cell with a GGI grading and the following I-V parameters without anti-reflective coating PCE 18%, V_{OC} 694 mV, J_{SC} 34 mA cm^{-2}, FF 76% was cleaved and a part of the freshly exposed cross section was coated with ~5 nm HfO_2. The measurements were conducted on the cross-section of both the HfO_2 coated and the uncoated device. The EBIC signal is normalized and drawn as color map overlay to the SEM signal allowing for qualitative comparison.

A larger extension of the collection function in the HfO_2 coated device was observed, similar to what has been reported for Al_2O_3 [22]. It appears likely that the same argument – that is an improved signal due to a reduced surface recombination on a p-type CIGS absorber – can be made for HfO_2 as reported for Al_2O_3. Thus, these findings can be interpreted by either a reduction of surface defect states, i.e. chemical passivation, or an upward band bending due to negative surface charge [13].

It is noted that from EBIC measurements it is neither unambiguous to discriminate the passivation mechanism of HfO_2 on the CIGS surface nor to quantify the effective charge density Q_{eff}. The most common method to address Q_{eff} would be C-V measurements on MIS structures [13,14]. The flat-band voltage can be attributed to a density of charges present in the insulating oxide layer. In our measurements a strong voltage-dependent hysteresis was found, i.e. the forward and backward measurements do not coincide. Therefore Q_{eff} could not be assessed (this is discussed in more detail in the SI, Fig. S1).

3.2. Application of HfO_2 in PV devices

In an attempt to assess the suitability of HfO_2 as a high bandgap passivation layer in CIGS solar cells a method for structuring the oxide layer was necessary. This is because already a few nanometer thick, unstructured HfO_2 layers showed a blocking behavior in the I-V curve at either CIGS/buffer or buffer/window interface (see I-V characterization below and in the SI).

3.2.1. Lithographic patterning

HCL was tested as a first structuring approach. Schematics for the process and an example of the obtained structuring are shown in Fig. 3. Openings of about 100 nm were obtained with an irregular spacing due to the surface roughness despite the photoresist deposition. HfO_2 was observed not to dissolve in alkaline conditions at pH ~11, hence solar cells could be produced with a conventional CBD-CdS buffer layer and ZnO/Al:ZnO window layer. With this configuration the standard device structure is kept similar to the reference device with a CIGS/CdS interface present only in the openings of the HfO_2 layer. Keeping the CdS as additional buffer layer, thus avoiding a CIGS/ZnO interface, allows a direct comparison of the HfO_2-passivated and the reference device.

Fig. 4 shows the I-V characteristics of devices comprising the same absorber layer but with a different surface treatment of the CIGS prior to the CBD-CdS deposition. HfO_2 layers with a thickness of about 10 nm were structured by HCL with different SF_6 etching times (1–4 min), to test which conditions are necessary to successfully create openings in the HfO_2. Already for the shortest sputtering time a structuring of HfO_2 was achieved, since a photodiode-like I-V curve was obtained which would otherwise not be expected even for a HfO_2 thickness as low as 3 nm (Fig. 4). The PCE of these cells, however, is far inferior to the reference device. Prolonged SF_6 sputtering seems to further negatively

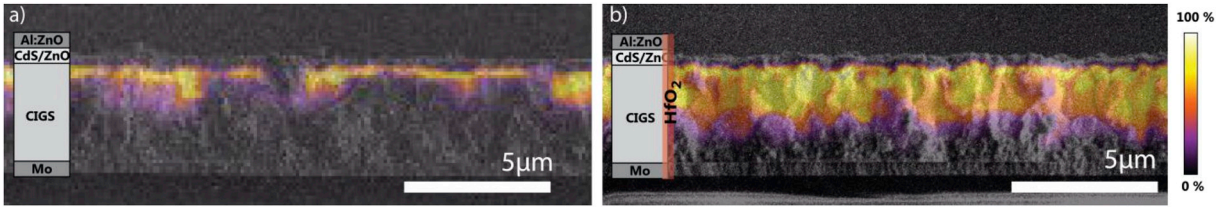

Fig. 2. SE micrograph with the EBIC signal overlaid as color map on a cleaved CIGS (CGI = 0.85, GGI = 0.4, graded) solar cell without and with ~5 nm HfO_2 coating. The acceleration voltage and beam current were 5 keV and 10–20 pA (measured with a faraday cup). The EBIC signal is normalized with the lower signal cutoff at the background level. (For interpretation of the references to color in this figure legend, the reader is referred to the Web version of this article.)

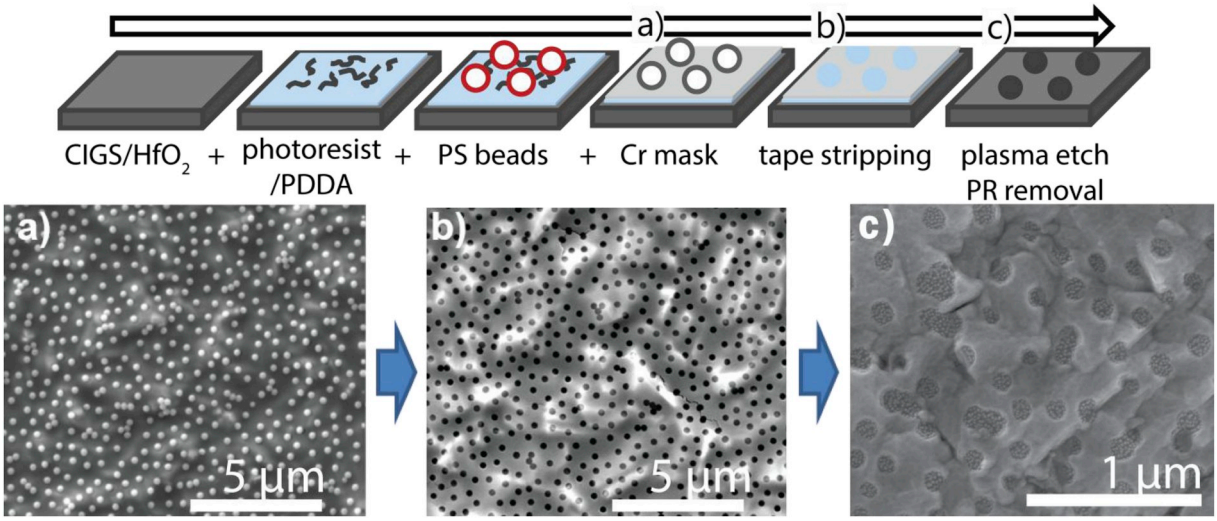

Fig. 3. HCL process for structuring of 100c HfO_2 on CIGS. SE micrographs of a) CIGS/HfO_2/photoresist (PR)/PS beads/Cr, b) after removal of PS beads by tape stripping and c) the final patterned oxide layer after a 2-step plasma etching of PR and HfO_2 and PR removal.

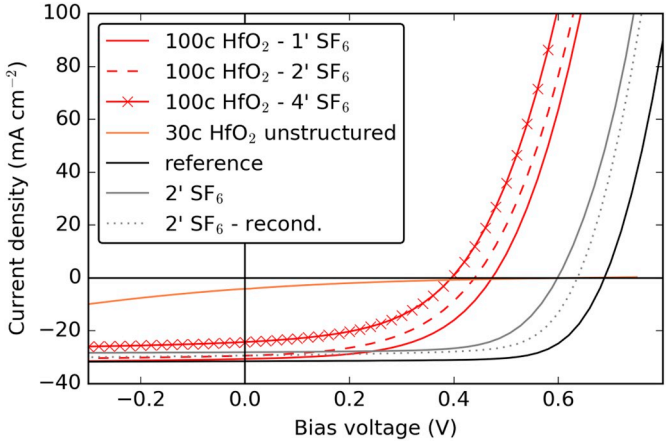

Fig. 4. J–V curves of SLG/SiO_x/Mo/CIGS/(HfO_2)/CdS/ZnO/Al:ZnO devices (CGI = 0.86, GGI = 0.41, graded) where the HfO_2 layer (100c) is patterned by HCL with SF_6 plasma for 1, 2, 4 min. In addition also one sample with an unstructured thin HfO_2 (30c) is added to visualize its current blocking behavior. The reference device employs the same absorber layer but was neither coated with HfO_2 nor exposed to plasma. For comparison, to see the detrimental effect of the plasma alone, two uncoated samples (without HfO_2) were exposed to 2 min SF_6 plasma after H_2O rinsing the absorber, one of which was further annealed in Se atmosphere prior to CdS CBD to recondition the surface (recond.).

impact all device parameters (V_{OC}, FF, J_{SC}) in a similar way. This could be assumed by an increased interface recombination introduced by the sputtering step on the CIGS surface or by a strong current blocking due to a non-optimal structuring geometry of the resistive HfO_2, or a combination of both effects. Simulations by Sozzi et al. [15] show a strong dependence of the I-V parameters (mostly V_{OC}) on the point contact width and pitch of a structured passivation layer. In their model this is attributed to the trade-off between the beneficial effect of surface defects passivation and the detrimental effect of series resistance. The pitch achieved by HCL (about 100–500 nm on average) was in the range where the simulations indicate a decreased V_{OC}. On this basis a performance loss is already expected in the HfO_2 coated devices presented in Fig. 4 due to the non-optimized structuring geometry.

However, to explain the decrease in PCE with prolonged SF_6 sputtering, an additional effect has to be responsible since the size of the openings and their distribution is expected to be similar and within the statistics of the 6 cells usually measured per sample (the intra-sample I-V parameter distribution is smaller than inter-sample, see Figure S 2). The most probable explanation is sputter damage of SF_6 on the CIGS surface causing an increase in the interface recombination. To validate this assumption, test structures were prepared where the bare (without HfO_2 coating) CIGS absorber after rinsing in H_2O was exposed to SF_6 plasma for two minutes. Annealing in Se atmosphere at 300–350 °C for 20 min was tested to recondition the surface after the plasma treatment. For the plasma treated device a by ~90 mV reduced V_{OC} is obtained which could be slightly recovered by the Se annealing. Since also J_{SC} is inferior by ~2 mA cm^{-2} these losses are most likely caused by an increased carrier recombination at the CIGS surface.

3.2.2. Template patterning

An alternative, faster and simpler bottom-up structuring approach was explored as follows. CIGS was dip-coated with NaCl from a saturated aqueous solution leaving various sized and randomly spaced NaCl crystallites on the surface. This procedure has the advantage that it can be repeated until the desired spacing is achieved by simply rinsing the surface in water and repeating the coating. Crystallite sizes of ~100 nm up to several µm were obtained. ALD-HfO_2 was then deposited on top of this template, which was then removed in an aqueous ultrasonic bath leaving the structured HfO_2 layers. In Fig. 5 an example is shown of about 4 or 6 nm HfO_2 deposited on a NaCl template prior and after water bath. A contrast in the SE image is clearly visible. Compared to HCL the structuring geometry is far less controlled with a non-periodic, more randomized pattern and openings of various sizes which is relatively far from the calculated optimum of regularly spaced openings of 10 nm with 50 nm pitch [15].

The PV device performance of a device with 100c ALD-HfO_2 (~10 nm) deposited on a graded CIGS absorber and structured with the NaCl based process is shown in Fig. 6. Comparable device efficiency to the reference device was achieved. The spread in the FF for the different cells was significantly higher than in the reference case and is attributed to the structuring process which was not optimized for cm^2-scale homogeneity. Compared to the HCL process the V_{OC} was not much affected since there was no harsh sputtering step which is the benefit of the template approach. EQE measurements revealed a slightly higher response in the blue wavelength region. This could be explained by a retarded growth of CdS on HfO_2 (see Figure S 3) leading to a reduced parasitic absorption of CdS. The I-V measurement showed an interesting non-ideality: Biasing the cell with the patterned HfO_2 in the dark at about +0.8 V (where the dark I-V current is 100 mA cm^{-2}) for 60s

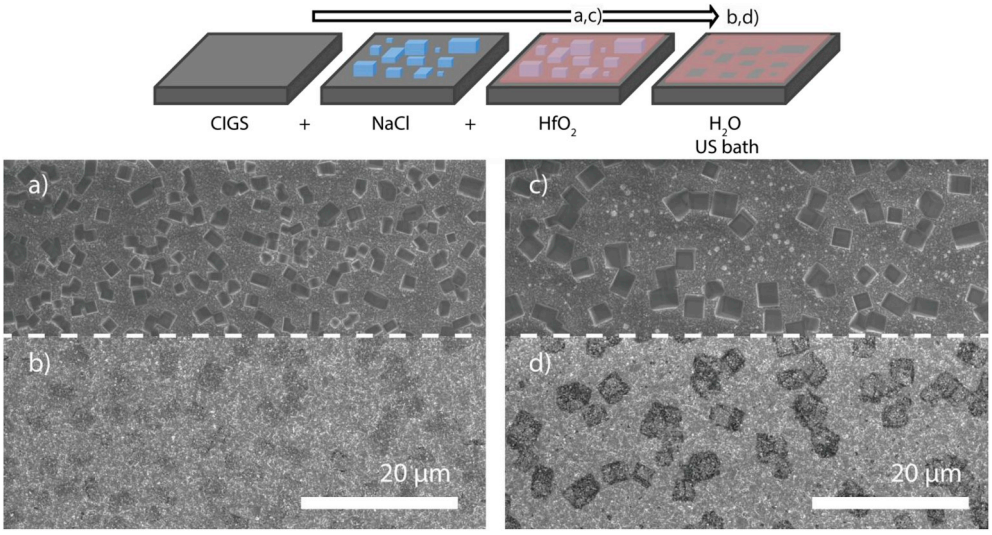

Fig. 5. SE micrograph of ~4 nm (a) and ~6 nm (c) HfO_2 deposited on CIGS/NaCl prior and after (b, d) sonication in water for 3 min.

prior to the voltage sweep showed to improve all I-V parameters, mostly FF leading to a gain in PCE of up to 0.9% absolute (In Fig. 6b this is shown for a device which shows this effect clearest). This effect was not seen in the reference device and the origin is unknown, but could be related to the hysteresis observed in the C-V measurements (Figure S 1) which is possibly caused by charge trap states.

3.2.3. HfO_2 at the CdS/ZnO interface

Another application of HfO_2 is investigated as intermediate HTR (highly transparent and resistive) layer in between the CdS and sputter deposited ZnO. The purpose here is to minimize sputtering damage during the window layer deposition. Especially for CdS it has been observed that the PV device performance degrades significantly if CdS is exposed to an O_2 plasma. More so if a thin (< 15 nm) CdS is applied and pin-holes in the layer are present, even a low power Ar plasma is influencing the FF (see Figure S 4). This is why the sputter-free deposition of the HRT layer is beneficial for when a thin CdS layer is employed [24,25]. Here, in a preliminary study the salt template

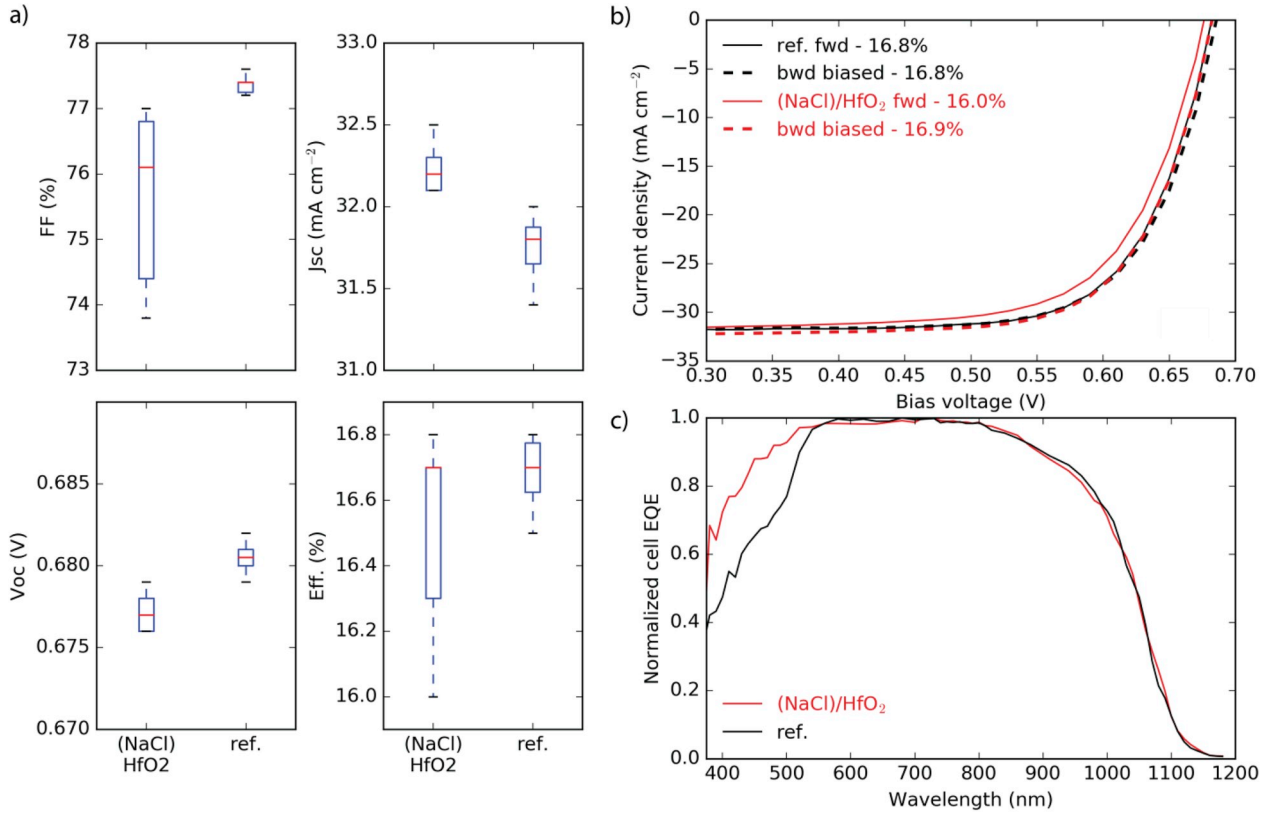

Fig. 6. a) Boxplot chart (6 best cells per sample) of the I-V parameters of CIGS (CGI = 0.85, GGI = 0.38, graded) solar cells with the structure SLG/SiO_x/Mo/CIGS/(HfO_2)/CdS/ZnO/Al:ZnO/grid(Ni,Al) where the HfO_2 (~10 nm) is structured via the NaCl template approach; The reference device employs no HfO_2 layer. b) J-V measurements of selected cells at different voltage sweep conditions: forward = [-0.75, 0.75] V, backward biased = pre-bias at +0.8V for 60s and sweep from [0.75, −0.75] V. c) corresponding normalized cell EQE.

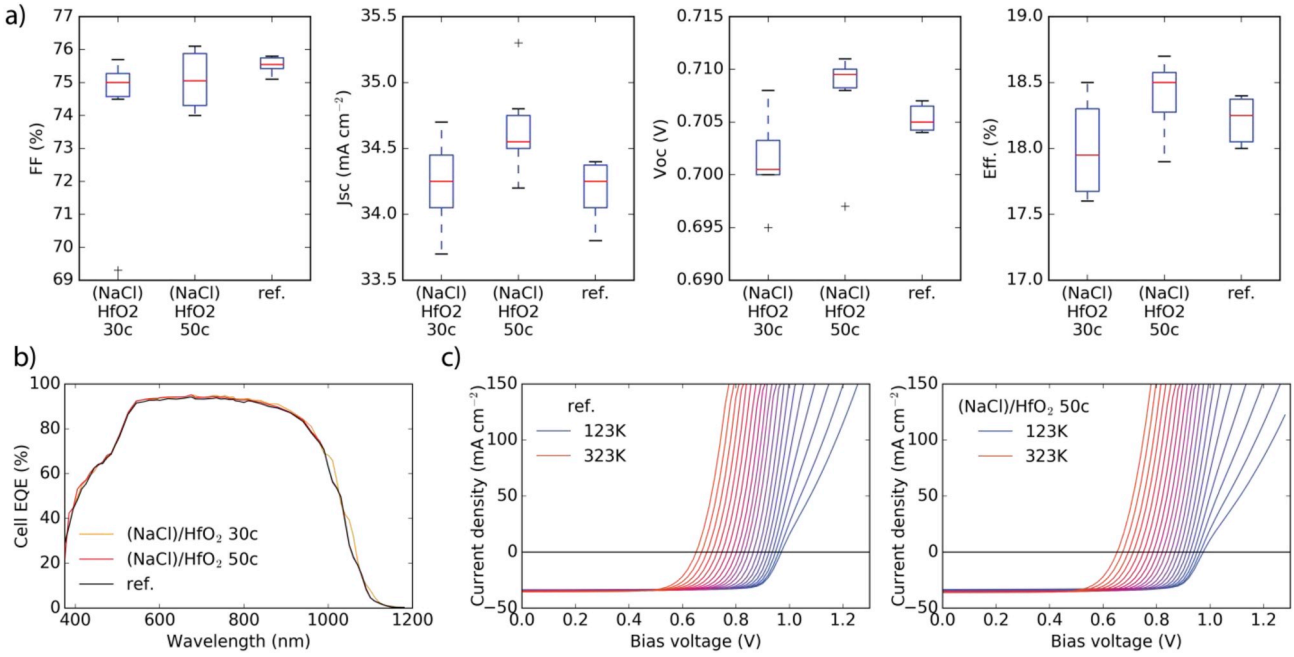

Fig. 7. a) Boxplot chart (6 best cells per sample) of the I-V parameters of CIGS (CGI = 0.88, GGI = 0.43, graded) solar cells with the structure SLG/SiO_x/Mo/CIGS/CdS/(HfO_2)/ZnO/Al:ZnO/grid(Ni,Al)/MgF_2 where the HfO_2 (30 or 50c = ~3 or 5 nm) is structured via the NaCl template approach; The reference device does not employ a HfO_2 layer. b,c) corresponding EQE (without MgF_2 ARC) and T-IV measurement from 123 to 323 K.

structuring was tested to pattern a thin HfO_2 layer on top of a ~50 nm CdS in combination with a standard ZnO/Al:ZnO window layer. The deposition temperature for HfO_2 in these experiments was reduced to 120 °C to avoid annealing effects of the SLG/SiO_x/Mo/CIGS/CdS structure. The influence of about 3 or 5 nm patterned HfO_2 on the I-V characteristics was found to be negligible. A larger spread of the FF values was again observed, but the median efficiency was similar to the reference structure (see Fig. 7a). Since the CdS growth was performed prior to the HfO_2 deposition the EQE measurements of the devices employing the HfO_2 layer were identical to the reference (Fig. 7b). Furthermore, temperature dependent I-V measurements (T-IV) showed no blocking effect at low temperatures (Fig. 7c). This experiment was repeated on a different absorber to improve statistics showing again comparable device efficiency for both structures (see Figure S 5). It can be concluded that thin layers of HfO_2, when deposited on CdS, are not introducing a significant carrier recombination and can be efficiently patterned with the salt template approach. For thicker HfO_2 layers (> 8 nm) the salt template structuring approach was found to be limited since the salt could not fully be removed anymore by simple ultrasound sonication in H_2O. Hence in solar cells, the FF is slightly decreasing with increasing the HfO_2 thickness in the investigated range (see Figure S 6 and S 7).

4. Conclusions

In the first part of this study ALD-HfO_2 was applied in test structures on the CIGS surface to assess its effects as a surface passivation layer. TRPL measurements showed a stable increase in the effective lifetime when HfO_2 is coated on the CIGS surface at elevated temperature. This effect could be reproduced on the uncoated sample annealed in Ar, however, it was found to be unstable for the uncoated absorber and a fast PL decay was again observed after storage in N_2 for a month. An improved carrier collection was observed in EBIC measurements due to the HfO_2 coating on the CIGS cross-section. The attempt to assign an oxide charge by C-V measurements on MIS structures was not successful due to a hysteresis effect, i.e. a dependence of the resulting C-V curve on the measurement conditions. In the second part the passivating effects of HfO_2 observed by TRPL and EBIC were tested in PV devices in a point contact concept. Two structuring methods for the highly resistive oxide were compared. A top down method (HCL) was found to severely degrade I-V parameters, which was related to the SF_6 plasma etching. The application of a bottom-up structuring approach of HfO_2 using a NaCl template showed more promising results although the structuring geometry was less defined. The device performance, however, was not improved by the introduction of HfO_2, at neither the CIGS/CdS or CdS/ZnO interface, when compared to the reference device.

Acknowledgement

The work has received funding from the Swiss Federal Office of Energy under contract No SI/501145-01 and the Swiss State Secretariat for Education, Research and Innovation (SERI) under contract No 15.0158. The work has received support from the European Union's Horizon 2020 research and innovation programme under grant agreement No 641004 (Sharc25).

Appendix A. Supplementary data

Supplementary data to this article can be found online at https://doi.org/10.1016/j.solmat.2019.03.009.

References

[1] A. Chirila, P. Reinhard, F. Pianezzi, P. Bloesch, A.R. Uhl, C. Fella, L. Kranz, D. Keller, C. Gretener, H. Hagendorfer, D. Jaeger, R. Erni, S. Nishiwaki, S. Buecheler, A.N. Tiwari, Potassium-induced surface modification of Cu(In,Ga)Se-2 thin films for high-efficiency solar cells, Nat. Mater. 12 (2013) 1107–1111.

[2] Press Release: Solar frontier achieves world record thin-film solar cell efficiency of 23.35%, http://www.solar-frontier.com/eng/news/2019/0117_press.html , Accessed date: 17 January 2019.

[3] P. Jackson, R. Wuerz, D. Hariskos, E. Lotter, W. Witte, M. Powalla, Effects of heavy alkali elementsin Cu(In,Ga)Se-2 solar cells with efficiencies up to 22.6%, Phys Status Solidi-R 10 (2016) 583–586.

[4] N. Naghavi, D. Abou-Ras, N. Allsop, N. Barreau, S. Bucheler, A. Ennaoui, C.H. Fischer, C. Guillen, D. Hariskos, J. Herrero, R. Klenk, K. Kushiya, D. Lincot, R. Menner, T. Nakada, C. Platzer-Bjorkman, S. Spiering, A.N. Tiwari, T. Torndahl, Buffer layers and transparent conducting oxides for chalcopyrite Cu(In,Ga)(S,Se)(2) based thin film photovoltaics: present status and current developments, Prog Photovoltaics 18 (2010) 411–433.

[5] J. Schmidt, A. Merkle, R. Brendel, B. Hoex, M.C.M. van de Sanden, W.M.M. Kessels, Surface passivation of high-efficiency silicon solar cells by atomic-layer-deposited Al2O3, Prog Photovoltaics 16 (2008) 461–466.
[6] A. Morato, B. Vermang, H. Goverde, E. Cornagliotti, G. Meneghesso, J. John, J. Poortmans, Electrical characterization of ALD Al2O3-HfO2 and PECVD Al2O3 passivation layers for p-type CZ-Silicon PERC solar cells, 2012 38th Ieee Photovoltaic Specialists Conference, Pvsc, 2012, pp. 1077–1082.
[7] D.K. Simon, P.M. Jordan, T. Mikolajick, I. Dirnstorfer, On the control of the fixed charge densities in Al2O3-based silicon surface passivation schemes, Acs Appl Mater Inter 7 (2015) 28215–28222.
[8] D. Ledinek, O. Donzel-Gargand, M. Skold, J. Keller, M. Edoff, Effect of different Na supply methods on thin Cu(In,Ga)Se-2 solar cells with Al2O3 rear passivation layers, Sol. Energy Mater. Sol. Cell. 187 (2018) 160–169.
[9] D. Ledinek, P. Salome, C. Hagglund, U. Zimmermann, M. Edoff, Rear contact passivation for high bandgap Cu(in,Ga)Se-2 solar cells with a flat Ga profile, Ieee Journal of Photovoltaics 8 (2018) 864–870.
[10] B. Vermang, J.T. Watjen, V. Fjallstrom, F. Rostvall, M. Edoff, R. Gunnarsson, I. Pilch, U. Helmersson, R. Kotipalli, F. Henry, D. Flandre, Highly reflective rear surface passivation design for ultra-thin Cu(In,Ga) Se-2 solar cells, Thin Solid Films 582 (2015) 300–303.
[11] P.M.P. Salome, B. Vermang, R. Ribeiro-Andrade, J.P. Teixeira, J.M.V. Cunha, M.J. Mendes, S. Haque, J. Borme, H. Aguas, E. Fortunato, R. Martins, J.C. Gonzalez, J.P. Leitao, P.A. Fernandes, M. Edoff, S. Sadewasser, Passivation of interfaces in thin film solar cells: understanding the effects of a nanostructured rear point contact layer, Advanced Materials Interfaces 5 (2018).
[12] S. Choi, Y. Kamikawa, J. Nishinaga, A. Yamada, H. Shibata, S. Niki, Lithographic fabrication of point contact with Al2O3 rear-surface-passivated and ultra-thin Cu (In,Ga)Se-2 solar cells, Thin Solid Films 665 (2018) 91–95.
[13] R. Kotipalli, O. Poncelet, G. Li, Y. Zeng, L.A. Francis, B. Vermang, D. Flandre, Addressing the impact of rear surface passivation mechanisms on ultra-thin Cu (In,Ga)Se-2 solar cell performances using SCAPS 1-D model, Sol. Energy 157 (2017) 603–613.
[14] S. Garud, N. Gampa, T.G. Allen, R. Kotipalli, D. Flandre, M. Batuk, J. Hadermann, M. Meuris, J. Poortmans, A. Smets, B. Vermang, Surface passivation of CIGS solar cells using gallium oxide, Phys. Status Solidi (2018) 215.
[15] G. Sozzi, S. Di Napoli, R. Menozzi, B. Bissig, S. Buecheler, A.N. Tiwari, Impact of front-side point contact/passivation geometry on thin-film solar cell performance, Sol. Energy Mater. Sol. Cell. 165 (2017) 94–102.
[16] A. Hultqvist, T. Sone, S.F. Bent, Buffer layer point contacts for CIGS solar cells using nanosphere lithography and atomic layer deposition, Ieee Journal of Photovoltaics 7 (2017) 322–328.
[17] B. Vermang, V. Fjallstrom, X.D. Gao, M. Edoff, Improved rear surface passivation of Cu(in,Ga)Se-2 solar cells: a combination of an Al2O3 rear surface passivation layer and nanosized local rear point contacts, Ieee Journal of Photovoltaics 4 (2014) 486–492.
[18] J. Aarik, H. Mändar, M. Kirm, L. Pung, Optical characterization of HfO2 thin films grown by atomic layer deposition, Thin Solid Films 466 (2004) 41–47.
[19] A. Chirila, S. Buecheler, F. Pianezzi, P. Bloesch, C. Gretener, A.R. Uhl, C. Fella, L. Kranz, J. Perrenoud, S. Seyrling, R. Verma, S. Nishiwaki, Y.E. Romanyuk, G. Bilger, A.N. Tiwari, Highly efficient Cu(In,Ga)Se-2 solar cells grown on flexible polymer films, Nat. Mater. 10 (2011) 857–861.
[20] F. Pianezzi, P. Reinhard, A. Chirila, B. Bissig, S. Nishiwaki, S. Buecheler, A.N. Tiwari, Unveiling the effects of post-deposition treatment with different alkaline elements on the electronic properties of CIGS thin film solar cells, Phys. Chem. Chem. Phys. 16 (2014) 8843–8851.
[21] A. Koprek, O. Cojocaru-Miredin, R. Wuerz, C. Freysoldt, B. Gault, D. Raabe, Cd and impurity redistribution at the CdS/CIGS interface after annealing of CIGS-based solar cells resolved by atom probe tomography, Ieee Journal of Photovoltaics 7 (2017) 313–321.
[22] B. Bissig, C. Guerra-Nunez, R. Carron, S. Nishiwaki, F. La Mattina, F. Pianezzi, P.A. Losio, E. Avancini, P. Reinhard, S.G. Haass, M. Lingg, T. Feurer, I. Utke, S. Buecheler, A.N. Tiwari, Surface passivation for reliable measurement of bulk electronic properties of heterojunction devices, Small 12 (2016) 5339–5346.
[23] T.P. Weiss, R. Carron, M. Wolter, J. Loeckinger, E. Avancini, S. Siebentritt, S. Buecheler, A.N. Tiwari, Time-resolved photoluminescence on double graded Cu (In,Ga)Se2 – impact of front surface recombination and its temperature dependence, Sci. Technol. Adv. Mater. (2019), https://doi.org/10.1080/14686996.2019.1586583.
[24] J. Löckinger, S. Nishiwaki, T.P. Weiss, B. Bissig, Y.E. Romanyuk, S. Buecheler, A.N. Tiwari, TiO2 as intermediate buffer layer in Cu(In,Ga)Se-2 solar cells, Sol. Energy Mater. Sol. Cell. 174 (2018) 397–404.
[25] J. Löckinger, S. Nishiwaki, C. Andres, R. Erni, M.D. Rossell, Y.E. Romanyuk, S. Buecheler, A.N. Tiwari, ALD-Zn xTi yO as window layer in Cu(in,Ga)Se2 solar cells, ACS Appl. Mater. Interfaces 10 (2018) 43603–43609.